



# Hydrothermal synthesis and white light emission of cubic $\text{ZrO}_2:\text{Eu}^{3+}$ nanocrystals



Sanoujam Dhiren Meetei, Shougaijam Dorendrajit Singh \*

Department of Physics, Manipur University, Canchipur, Imphal 795 003, India

## ARTICLE INFO

### Article history:

Received 3 September 2013  
Received in revised form 16 October 2013  
Accepted 19 October 2013  
Available online 31 October 2013

### Keywords:

Hydrothermal  
White light  
Cubic zirconia  
Nanocrystal  
Photoluminescence

## ABSTRACT

Production of white light has been a promising area of luminescence studies. In this work, white light emitting nanocrystals of cubic zirconia doped with  $\text{Eu}^{3+}$  are synthesized by hydrothermal technique. The dopant  $\text{Eu}^{3+}$  is used to stabilize crystalline phase to cubic and at the same time to get red counterpart of the white light. The synthesis procedure is simple and precursor required no further annealing for crystallization. X-ray diffraction patterns show the crystalline phase of  $\text{ZrO}_2:\text{Eu}^{3+}$  to be cubic and it is confirmed by Fourier Transform Infrared spectroscopy. From transmission electron microscopy images, size of the crystals is found to be  $\sim 5$  nm. Photoluminescence emission spectrum of the sample, on monitoring excitation at  $\text{O}^{2-}-\text{Eu}^{3+}$  charge transfer state shows broad peak due to  $\text{O}^{2-}$  of the zirconia and that of  $\text{Eu}^{3+}$  emission. *Commission Internationale de l'éclairage* co-ordinate of this nanocrystal (0.32, 0.34) is closed to that of the ideal white light (0.33, 0.33). Correlated color temperature of the white light (5894 K) is within the range of vertical daylight. Lifetime (1.32 ms) corresponding to  ${}^3\text{D}_0$  energy level of the  $\text{Eu}^{3+}$  is found to be far longer than conventional red counterparts of white light emitters. It suggests that the  $\text{ZrO}_2:\text{Eu}^{3+}$  nanocrystals synthesized by hydrothermal technique may find applications in simulating the vertical daylight of the Sun.

© 2013 Elsevier B.V. All rights reserved.

## 1. Introduction

Since time immemorial human being has been mimicking the Mother Nature. As a part of it, lot of research is going on to mimic the Sun light artificially through the fabrication of white light emitters [1–8]. White light can be fabricated by mixing individual red, green and blue (RGB) lights. However, it is expensive in terms of both equipment and energy consumption [1,2]. Therefore, emission of white light from a phosphor is of prime importance due to growing concern about energy saving and environmental friendliness [3]. Furthermore, white light production from a phosphor is simpler and cheaper than a complex RGB system [5]. In view of these facts, white light emitting phosphors (WLEPs) have attracted much attention in the recent years for application in various forms of lighting devices such as white LEDs [6–10].

Zirconia is an attractive material in both fundamental and application-oriented research. It is well known for low thermal conductivity, high melting point, high thermal and mechanical resistance. It is used as an ideal medium for fabrication of highly luminescent material due to its high refractive index, low phonon energy, high chemical and photochemical stability [11–16].

Recently, there has been an increasing interest in the application of  $\text{ZrO}_2$  nanocrystals due to their enhanced luminescent properties associated with their small size [11]. Therefore, extensive amount of works have been reported on the properties of bulk and nanocrystalline  $\text{ZrO}_2$  of different crystalline phases [11–17]. Even though, cubic phase is the most desirable phase of zirconia [17], to the best knowledge of the authors, no report has been found for production of white light from cubic  $\text{ZrO}_2:\text{Eu}^{3+}$ . Generally, zirconia has three crystalline phases, viz., monoclinic (<1443 K), tetragonal (1443–2643 K) and cubic (>2643 K) [8,11–13]. In fact, as the crystallite size decreases, the crystalline structure transform to a structure with higher symmetry. Therefore, it is our desire to synthesized zirconia at low dimension to get high symmetric cubic phase. Interestingly, in order to fabricate zirconia devices, it is necessary to lock the material wholly or partially into the cubic phase by a use of stabilizing agent [18]. Meanwhile, it is also found in reports that there is lack of red counterpart in the WLEPs and  $\text{Eu}^{3+}$  is a potential candidate to rectify this problem [19,20]. Therefore, it will be a motivating task if one can synthesize the nanocrystals of cubic zirconia by  $\text{Eu}^{3+}$  doping; at the same time  $\text{Eu}^{3+}$  is used as the stabilizing agent and red counterpart of white light. Most of the reports for the synthesis of WLEPs used solid state reaction. However, such reaction suffers from serious drawbacks like reactants should mix to a homogenous system, high viscosity in reactant system, unsuitable for solvent assisted chemical reactions,

\* Corresponding author. Tel.: +91 385 2435080; fax: +91 385 2435145.

E-mail addresses: [sdmdhiren@gmail.com](mailto:sdmdhiren@gmail.com) (S.D. Meetei), [dorendrajit@yahoo.co.in](mailto:dorendrajit@yahoo.co.in) (S.D. Singh).

among others [21,22]. Therefore, most of the reported WLEPs are complex in nature and consequently complex in synthesis [7,19]. As a result, simple hydrothermal techniques for synthesis of WLEPs are expected to prefer over solid state reaction. It is found in the reports that hydrothermal technique of material synthesis has advantages of high purity, narrow particle size distribution, low crystallization temperature, high crystallinity, high degree of precipitation, easy to control powder composition, ecological friendly, etc., among others [23–26]. Meanwhile, from the synthesis and characterization point of views, single dopant phosphors are preferred for production of white light. Unfortunately, phosphors with multiple dopants are usually found in the reports for the same [27,28].

In view of all these facts, present work is devoted to the production of white light from single ion i.e.  $\text{Eu}^{3+}$  doped cubic  $\text{ZrO}_2$  nanocrystals through hydrothermal technique. To our best knowledge there are no reports for the production of white light from cubic  $\text{ZrO}_2:\text{Eu}^{3+}$  nanocrystals synthesized by hydrothermal technique. In the present work, nanocrystalline cubic  $\text{ZrO}_2:\text{Eu}^{3+}$  are successfully synthesized by hydrothermal technique for production of white light. The sample is characterized by HRTEM (high resolution transmission electron microscopy), XRD (x-ray diffraction), FT-IR (Fourier transform infra-red) and photoluminescence (PL) spectroscopy. From the PL emission data, CIE (*Commission Internationale de l'éclairage*) chromaticity co-ordinates and consequently CCT (correlated color temperature) are calculated. PL decay lifetime corresponding to  $^5\text{D}_0$  energy level of  $\text{Eu}^{3+}$  is also determined from the  $\text{ZrO}_2:\text{Eu}^{3+}$  nanocrystals.

## 2. Experimental section

### 2.1. Hydrothermal synthesis

For synthesis of  $\text{ZrO}_2:\text{Eu}^{3+}$ , zirconium (IV) oxychloride octahydrate,  $\text{ZrOCl}_2 \cdot 8\text{H}_2\text{O}$  (Riedel-de Haën,  $\geq 99.5\%$ ) (250 mg) was added to distilled water (Millipore) (25 ml) and allowed to dissolve with a magnetic stirrer at 1200 rpm (3 min). Then, europium (III) nitrate pentahydrate,  $\text{Eu}(\text{NO}_3)_3 \cdot 5\text{H}_2\text{O}$ , (Aldrich, 99.9%) (6.8 mg) was added to the solution and continued stirring (15 min). Subsequently, urea,  $\text{CH}_4\text{N}_2\text{O}$  (Merck,  $\geq 99.9\%$ ) (1000 mg) was added to the solution. Then, the whole solution was transferred to a 250 ml vertical Teflon-liner, autoclave. Next, the autoclave is kept in a hot air oven of constant crystallization temperature (433 K) for 24 h. Then, the autoclave was allowed to cool at room temperature naturally. On opening the autoclave, white dense precipitates are obtained in the background of a clear liquid. The white precipitate thus obtained was collected in a tube and then centrifuged at 10,000 rpm (5 min). After this, the precipitate was washed with distilled water (5 times) and then with acetone (3 times). Finally, it was dried at room temperature and ground to form powder. Similar procedure is used for synthesis of undoped sample.

### 2.2. Characterization

XRD data of the samples are recorded in PANalytical instrument (40 kV and 30 mA). The wavelength used is that of  $\text{Cu K}\alpha$  (1.54060 Å). HRTEM images and SAED (selected area electron diffraction) rings are recorded using JEM-2100 microscope (JEOL) (200 kV). FTIR spectra are recorded in MB102 spectrometer (BOMEN). PL emission, excitation spectra and lifetime are obtained from LS55 Luminescence Spectrometer (Perkin Elmer). All the measurements are recorded at room temperature.

## 3. Results and discussion

### 3.1. HRTEM and SAED

Fig. 1a and b show HRTEM images of  $\text{ZrO}_2:\text{Eu}^{3+}$  nanocrystals. The images show size of the crystals to be  $\sim 5$  nm. Fig. 1c shows faint rings of SAED (selected area electron diffraction). The faint rings reveal the small size of the crystals. Interplaner spacings,  $d_{hkl}$ , corresponding to the four main rings at 3.38, 3.92, 5.52 and 6.45 1/nm are calculated. Respectively, they are found to be 2.96, 2.55, 1.81 and 1.55 Å. It agrees with the interplaner spacing of (111),

(200), (220) and (311) corresponding to the cubic zirconia (ICDD Ref. Code: 00-049-1642). Fig. 1d shows the enlarged view of a portion of Fig. 1a. It shows the interplaner spacing, 2.96 Å, which corresponds to (111) planes of the cubic zirconia. The HRTEM images and SAED rings confirms that the precursor is crystalline and the sample required no further heat treatment for crystallization.

### 3.2. XRD

Fig. 2 shows XRD patterns of the  $\text{ZrO}_2$  and  $\text{ZrO}_2:\text{Eu}^{3+}$  nanocrystals. Due to nanocrystalline nature, the patterns show peak broadening. Analysis of the patterns by PANalytical's X'Pert High Score Search Match show that undoped  $\text{ZrO}_2$  present both  $P21/c$  monoclinic (ICDD Ref. Code No. 01-086-1451) and  $P42/nmc$  tetragonal (ICDD Ref. Code No. 01-079-1770) phases. However, the pattern of  $\text{ZrO}_2:\text{Eu}^{3+}$  shows  $Fm-3m$  cubic phase (ICDD Ref. Code No. 00-049-1642). The patterns for the said codes are also shown in the Fig. 2. From the XRD patterns, it is clearly observed that the monoclinic and tetragonal phases of undoped  $\text{ZrO}_2$  is stabilized to cubic phase when  $\text{Eu}^{3+}$  is introduced in the host zirconia. This can be explained on the line of substitution of  $\text{Zr}^{4+}$  by  $\text{Eu}^{3+}$  thereby creating  $\text{O}^{2-}$  vacancy. The appropriate place for  $\text{Eu}^{3+}$  in the host  $\text{ZrO}_2$  is  $\text{Zr}^{4+}$  site and charge difference is compensated by an oxygen vacancy ( $\text{O}^{2-}$ ) when  $\text{Eu}^{3+}$  substituted  $\text{Zr}^{4+}$ . Since, oxygen vacancy serves to compensate the difference in charge between  $\text{Eu}^{3+}$  and  $\text{Zr}^{4+}$ , one oxygen vacancy is evolved for every two  $\text{Zr}^{4+}$  replaced by two  $\text{Eu}^{3+}$  ions [8,11].

### 3.3. FT-IR

The XRD patterns of tetragonal and cubic phases of zirconia are similar. Therefore, the FT-IR spectra of the samples are recorded to substantiate the XRD patterns. To observe the characteristic band due to  $\text{ZrO}_2$ , FT-IR spectra are shown within the finger print region, 300–900  $\text{cm}^{-1}$  (Fig. 3). The spectrum of the  $\text{ZrO}_2$  where both monoclinic and tetragonal phases exist show bands at 357, 418, 455, 507, 577 and 728  $\text{cm}^{-1}$ . The bands at 357, 418, 507 and 728  $\text{cm}^{-1}$  are characteristic of the monoclinic phase ascribed to the  $5\text{A}_u$  and  $6\text{B}_u$  active modes. While the bands at 455 and 577  $\text{cm}^{-1}$  are attributed to Zr–O stretching of the tetragonal zirconia [8,29]. However,  $\text{ZrO}_2:\text{Eu}^{3+}$  shows no band due to tetragonal phase. Rather it shows a broad band at 447  $\text{cm}^{-1}$  and a shoulder at 615  $\text{cm}^{-1}$ . This is consistent with the statement that only one fundamental mode is active in cubic zirconia [30]. Thus, the  $\text{ZrO}_2:\text{Eu}^{3+}$  is confirmed to be cubic in phase.

### 3.4. PL excitation and emission

Photoluminescence excitation and emission spectra of the cubic  $\text{ZrO}_2:\text{Eu}^{3+}$  nanocrystals are shown in Fig. 4. On monitoring the emission at 609 nm corresponding to structurally sensitive,  $^5\text{D}_0 \rightarrow ^7\text{F}_2$ , electric dipole transition of  $\text{Eu}^{3+}$ , the excitation spectrum shows a peak at 244 nm and a hump at 260 nm. The peak (244 nm) is attributed to  $\text{O}^{2-}-\text{Eu}^{3+}$  charge transfer originating from electronic transitions from 2p orbital of  $\text{O}^{2-}$  to 4f orbital of the  $\text{Eu}^{3+}$  [8,17]. While, the hump at 260 nm is attributed to the presence of oxygen vacancy arises due to substitution of  $\text{Zr}^{4+}$  by  $\text{Eu}^{3+}$  described above.

On monitoring the excitation at the charge transfer state, 244 nm, a broad peak centered at 486 nm and well known  $\text{Eu}^{3+}$  peaks are observed. The peak at 486 nm is attributed to  $\text{O}^{2-}$  vacancy is observed from the XRD and PL excitation spectrum. The peak at 592 nm is attributed to magnetic dipole transition,  $^5\text{D}_0 \rightarrow ^7\text{F}_1$ , of  $\text{Eu}^{3+}$ . On the other hand, the peak at 609 nm is attributed to structurally sensitive electric dipole transition,  $^5\text{D}_0 \rightarrow ^7\text{F}_2$ , of  $\text{Eu}^{3+}$ .

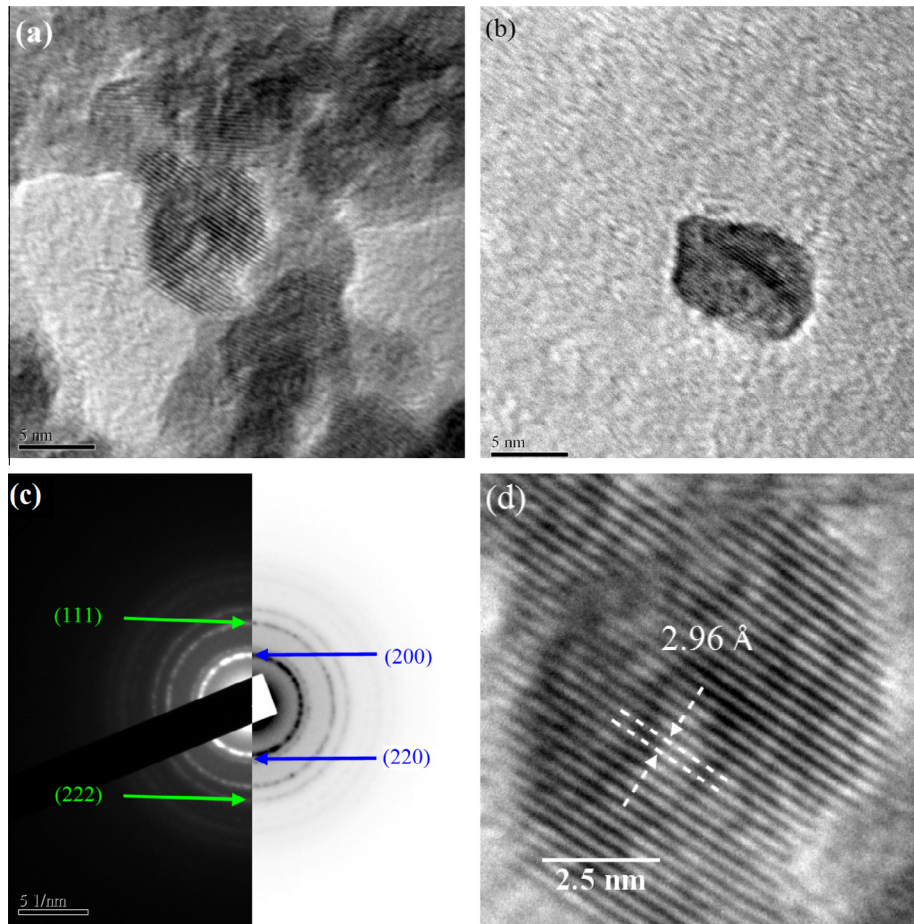


Fig. 1. (a and b) HRTEM images, (c) SAED rings and (d) enlarged view of (a) showing interplaner spacing of the cubic  $\text{ZrO}_2:\text{Eu}^{3+}$  nanocrystals.

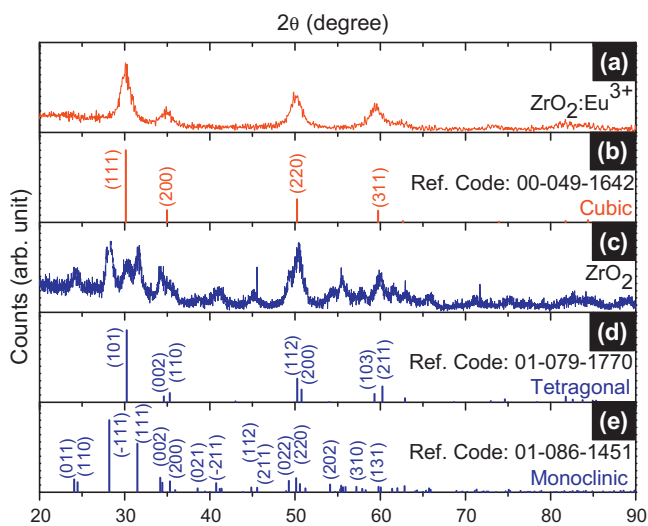


Fig. 2. XRD patterns of the (a) cubic  $\text{ZrO}_2:\text{Eu}^{3+}$ , (b) ICDD Ref. Code: 00-049-1642, (c)  $\text{ZrO}_2$  (monoclinic + tetragonal), (d) ICDD Ref. Code: 01-079-1770 and (e) ICDD Ref. Code: 01-086-1451.

Relative intensity of the electric (E) and magnetic (M) dipole transitions (i.e. E/M), also called *asymmetry ratio*, strongly depend on the local symmetry of  $\text{Eu}^{3+}$ . The asymmetry ratio of the sample is 1.04. This value is lower than that of reported tetragonal phase. It suggests that the sample have higher symmetry than tetragonal phase i.e. the sample is cubic [32,33].

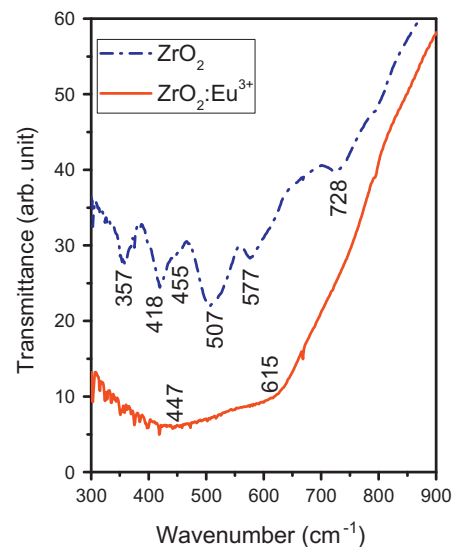


Fig. 3. FT-IR spectra of  $\text{ZrO}_2$  (monoclinic + tetragonal) and  $\text{ZrO}_2:\text{Eu}^{3+}$  (cubic) nanocrystals.

### 3.5. CIE chromaticity and CCT

The broad peak of the vacancy state and  $\text{Eu}^{3+}$  peaks within the visible range (400–700 nm) disclose that this nanocrystal will emit

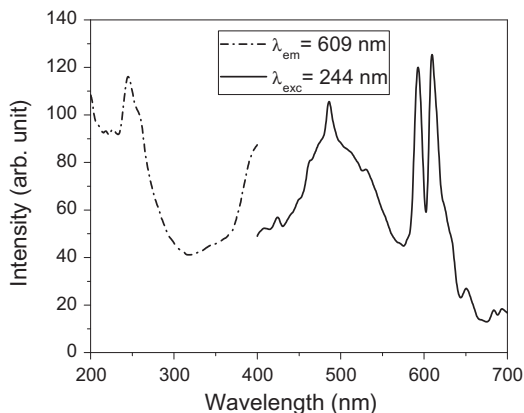


Fig. 4. PL excitation and emission spectra of the cubic  $\text{ZrO}_2:\text{Eu}^{3+}$  nanocrystals.

white light. Therefore, *Commission Internationale de l'éclairage* (CIE) co-ordinate of the nanocrystal is calculated. The CIE co-ordinate is found to be (0.32, 0.34), which is closed to that of the ideal white light (0.33, 0.33). The emission of white light from this nanocrystal can be attributed to comparable intensities of the vacancy and  $\text{Eu}^{3+}$  emissions in the visible range of electromagnetic spectrum. To identify technical applicability of this white light, *correlated color temperature* (CCT) is determined from CIE coordinate. Fig. 5 shows Planckian locus in the CIE chromaticity diagram for calculation of CCT. The lines perpendicular to the Planckian locus is called isotherm lines and they nearly converge towards a point on the chromaticity diagram. A slope line can be drawn by joining the point and the coordinate (x,y) in quest. With this slope, CCT at the coordinate (x,y) can be calculated by using the approximation:

$$\text{CCT}(x, y) = -449n^3 + 3525n^2 - 6823.3n + 5520.33 \quad (1)$$

Where  $n = (x - x_e)/(y - y_e)$  is inverse of the slope line and ( $x_e = 0.33$ ,  $y_e = 0.19$ ) is the convergent point [34,35]. The calculated CCT value of this nanocrystal is 5894 K which corresponds to vertical daylight

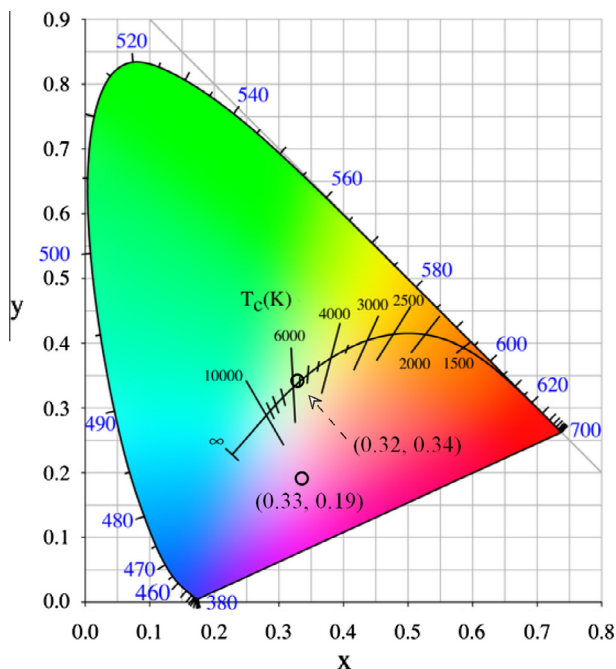


Fig. 5. CIE diagram showing the coordinate (0.32, 0.34), Planckian locus and point of convergence (0.33, 0.19).

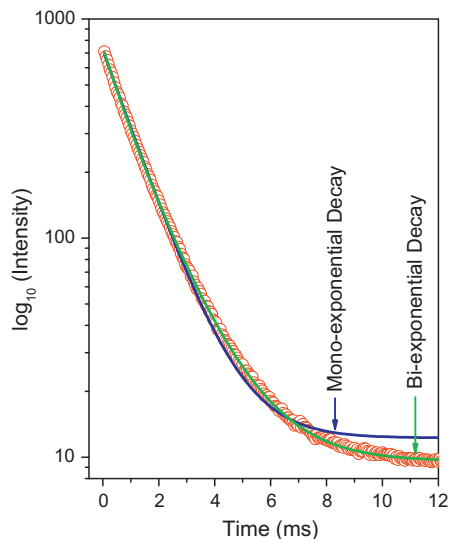


Fig. 6. PL decay curves result from  $^5\text{D}_0$  energy level of  $\text{Eu}^{3+}$ .

(5500–6000 K) [34]. Therefore, the white light emitted from this nanocrystal can be used for artificial production of vertical daylight of the Sun.

### 3.6. PL lifetime

Fig. 6 shows the PL decay curve of  $^5\text{D}_0$  energy level of  $\text{Eu}^{3+}$ . The decay curve is recorded on monitoring the excitation and emission wavelengths at 244 and 609 nm respectively. The figure is shown in  $\log_{10}$  (Intensity) vs. time to observe the difference in mono-exponential and bi-exponential fittings vividly. From the figure it is clearly observed that bi-exponential decay fits better than mono-exponential decay. The goodness of fit for bi-exponential decay fit is 0.9999. While the goodness of fit for mono-exponential decay fit is 0.9992. The fitted bi-exponential equation is of the form:

$$I = I_1 \exp(-t/\tau_1) + I_2 \exp(-t/\tau_2) + I_0 \quad (2)$$

where  $I_1$  and  $I_2$  are intensities at two different values of time ( $t$ ) i.e.,  $\tau_1$  and  $\tau_2$ ; and  $I_0$  is the offset. The validity of bi-exponential decay suggests that the PL decay is associated with two different probabilities of decay [36]. From the fitting the values of  $\tau_1$  and  $\tau_2$  are found to be 0.78 and 1.53 ms corresponding to  $I_1$  and  $I_2$  values of 314 (43%) and 415 (57%) respectively. Slow component (1.53 ms) results from the  $\text{Eu}^{3+}$  in the inner core of the crystals and the fast component (0.78 ms) results from the surface  $\text{Eu}^{3+}$ .

Assuming the shape of the nanocrystals as spherical, average lifetime,  $\tau_{ave}$  is calculated by using the equation [8]:

$$\tau_{ave} = (I_1 \tau_1^2 + I_2 \tau_2^2) / (I_1 \tau_1 + I_2 \tau_2) \quad (3)$$

The calculated  $\tau_{ave}$  is found to be 1.32 ms. This value is six order of magnitudes longer than lifetime of red counterpart of conventional WLEPs [37]. It suggests that problem of short lifetime encountered by red counterpart of conventional WLEPs can be rectified by the cubic  $\text{ZrO}_2:\text{Eu}^{3+}$  nanocrystals synthesized by hydrothermal technique.

## 4. Conclusion

Our results open an efficient way to produce vertical daylight of the Sun artificially. The white light emitting cubic  $\text{ZrO}_2:\text{Eu}^{3+}$  nanocrystal can be synthesized by hydrothermal technique. The precursor is crystalline in nature and the crystallization temperature is

low. Cubic phase observed from XRD result is substantiated by FT-IR spectra and PL. TEM images show the size of the crystals to be ~5 nm. The dopant  $\text{Eu}^{3+}$  is used to stabilize the crystalline phase to cubic and at the same time to get red counterpart of the white light. The broad PL emission due to oxygen vacancy combines with that of the dopant to give white light from the sample. The longer lifetime corresponding to red counterpart of the sample may resolve the problem of short lifetime faced by conventional WLEPs. The vertical daylight emission from this nanocrystal suggests that the nanocrystal may find uses in mimicking daylight of the Sun. By fabricating LEDs from this nanocrystal, electronic flash, lightings of theater and opera may enter to a new generation.

### Acknowledgments

One of the author, S. Dhiren Meetei thanks Council of Scientific & Industrial Research (CSIR), New Delhi, India for awarding Senior Research Fellowship (File No.: 09/476/ (0069)/2013/EMR-1). The authors wish to thank SAIF, NEHU, Shillong, Meghalaya, India for providing TEM facility.

### References

- [1] Daylight, Wikipedia. <<http://en.wikipedia.org/wiki/Daylight>>. (accessed 03.09.2013).
- [2] E.F. Schubert, J.K. Kim, *Science* 308 (2005) 1274–1278.
- [3] P. Dai, X. Zhang, X. Li, G. Wang, C. Zhao, Y. Liu, *J. Lumin.* 131 (2011) 653–65625.
- [4] H. He, R. Fu, X. Song, D. Wang, J. Chen, *J. Lumin.* 128 (2008) 489–493.
- [5] Light-emitting diode. Wikipedia. <[http://en.wikipedia.org/wiki/Light-emitting\\_diode#Phosphor-based\\_LEDs](http://en.wikipedia.org/wiki/Light-emitting_diode#Phosphor-based_LEDs)>. (accessed 03.09.2013).
- [6] C.K. Chung, T.Y. Chen, C.W. Lai, *Scripta Mater.* 65 (2011) 432–435.
- [7] Y. Chen, M. Gong, G. Wang, Q. Su, *Appl. Phys. Lett.* 91 (2007) 071117.
- [8] S.D. Meetei, S.D. Singh, N.S. Singh, V. Sudarsan, R.S. Ningthoujam, M. Tyagi, S.C. Gadkari, R. Tewari, R.K. Vatsa, *J. Lumin.* 132 (2012) 537–544.
- [9] A.K. Parchur, A.I. Prasad, S.B. Rai, R.S. Ningthoujam, *Dalton Trans.* 41 (2012) 13810–13814.
- [10] R.S. Loitongbam, N.S. Singh, W.R. Singh, R.S. Ningthoujam, *J. Lumin.* 134 (2013) 14–23.
- [11] L. Kumari, W.Z. Li, J.M. Xu, R.M. Leblanc, D.Z. Wang, Y. Li, H. Guo, J. Zhang, *Cryst. Growth Des.* 9 (2009) 3874–3880.
- [12] R. Gillani, B. Ercan, A. Qiao, T.J. Webster, *Int. J. Nanomed.* 5 (2010) 1–11.
- [13] Y. Al-Khatatbeh, K.K.M. Lee, B. Kiefer, *Phys. Rev. B* 81 (2010) 214102.
- [14] E. De la Rosa, L.A. Diaz-Torres, P. Salas, R.A. Rodríguez, *Opt. Mater.* 27 (2005) 1320–1325.
- [15] D.E. Harrison, N.T. McLamed, E.C. Subbarao, *J. Electrochem. Soc.* 110 (1963) 23–28.
- [16] P. Ghosh, A. Patra, *Langmuir* 22 (2006) 6321–6327.
- [17] L. Chen, Y. Liu, Y. Li, *J. Alloys Comp.* 381 (2004) 266–271.
- [18] Zirconia-ZrO<sub>2</sub>, Zirconium Dioxide. The A to Z of materials. <<http://www.azom.com/Details.asp?ArticleID=133>>. (accessed 03.09.2013).
- [19] Y.N. Xue, F. Xiao, Q.Y. Zhang, *Spectrochim. Acta Part A* 78 (2011) 1445–1448.
- [20] Y.Q. Li, J.E.J. van Steen, J.W.H. van Krevel, *J. Alloys Comp.* 417 (2006) 273–279.
- [21] Dry media reaction. Wikipedia. <[http://en.wikipedia.org/wiki/Dry\\_media\\_reaction](http://en.wikipedia.org/wiki/Dry_media_reaction)>. (accessed 03.09.2013).
- [22] A.R. West, *Solid State Chemistry and Its Applications*, first ed., John Wiley and Sons, Singapore, 2005.
- [23] R. Piticescu, C. Monty, D. Millers, *Sens. Actuat. B* 109 (2005) 102–106.
- [24] L. Cristea, R.R. Piticescu, B. Popescu, M. Teleanu, *Metalurgija* 42 (2003) 99–102.
- [25] K. Byrappa, M. Yoshimura, *Handbook of Hydrothermal Technology*, first ed., Noyes Publications, New York, 2001.
- [26] N.S. Singh, R.S. Ningthoujam, G. Phaomei, S.D. Singh, A. Vinud, R.K. Vatsa, *Dalton Trans.* 41 (2012) 4404–4412.
- [27] M. Cocchi, J. Kalinowski, D. Virgil, V. Fattori, S. Develay, J.A.G. Williams, *Appl. Phys. Lett.* 90 (2007) 163508.
- [28] B.W. D'andrade, J. Brooks, V. Adamovich, M.E. Thompson, S.R. Forrest, *Adv. Mater.* 14 (2002) 10321036.
- [29] Joo, T. Yu, Y.W. Kim, H.M. Park, F. Wu, J.Z. Zhang, T. Hyeon, *J. Am. Chem. Soc.* 125 (2003) 6553–6557.
- [30] S.F. Wang, F. Gu, M.K. Lü, Z.S. Yang, G.J. Zhou, H.P. Zhang, Y.Y. Zhou, S.M. Wang, *Opt. Mater.* 28 (2006) 1222–1226.
- [31] A. Emeline, G.V. Kataeva, A.S. Litke, A.V. Rudakova, V.K. Ryabchuk, N. Serpone, *Langmuir* 14 (1998) 5011–5022.
- [32] K. Moon, I.M. Kwon, J.H. Jeong, C.K. Kim, S.S. Yi, P.S. Kim, H. Choi, J.H. Kim, *J. Lumin.* 122 (2007) 855–857.
- [33] S.D. Meetei, S.D. Singh, V. Sudarsan, *J. Alloys Comp.* 514 (2012) 174–178.
- [34] Color temperature. Wikipedia. <[http://en.wikipedia.org/wiki/Color\\_temperature](http://en.wikipedia.org/wiki/Color_temperature)>. (accessed 03.09.2013).
- [35] C.S. McCamy, *Color Res. Appl.* 17 (1992) 142–144.
- [36] T. Ninjbadgar, G. Garnweitner, A. Börger, L.M. Goldenberg, O.V. Sakhno, J. Stumpe, *Adv. Funct. Mater.* 19 (2009) 1819–1825.
- [37] S. Sapra, S. Mayilo, T.A. Klar, A.L. Rogach, J. Feldmann, *Adv. Mater.* 19 (2007) 569–572.